The International Archives of the Photogrammetry, Remote Sensing and Spatial Information Sciences, Volume XLIX-B2-2026
XXV ISPRS Congress 2026 “From Imagery to Understanding”, Commission II, 4–11 July 2026, Toronto, Canada

Railway parameter extraction with high-precision UAV-photogrammetry: a feasibility study

Lucas De Burggrave[1], Erkki Bartczak[1], Suzanna Cuypers[1], Jens Derdaele[2] and Maarten Bassier[1,*]

[1]Dept. of Civil Engineering, –Geomatics Section,
KU Leuven - Faculty of Engineering Technology, Ghent, Belgium

[2]Surveying Dept. – TUC RAIL, Brussels, Belgium
maarten.bassier@kuleuven.be

Keywords: Railway systems, Structure-from-Motion, 3D reconstruction, Point Clouds, CAD, UAV.

Abstract

This paper presents a feasibility study on the extraction of railway parameters from high-precision UAV photogrammetry. A two-stage methodology is adopted: first, point-cloud accuracy and rail-surface coverage are optimized through controlled laboratory and field acquisitions; second, the resulting point clouds are evaluated against the local precision requirements for railway parameter extraction. Laboratory tests show that the SfM workflow is intrinsically capable of sub-millimeter agreement under controlled conditions. In the field, standard nadir and higher-altitude flights proved insufficient to reconstruct the narrow rail-side geometry required for accurate gauge estimation. The best results were obtained by combining a 15 m nadir flight with additional side-looking images at 2.5 m and 5 m, yielding local fitted-surface RMS values down to 0.25 mm and about 0.37 mm on the rail running surface.

Although the best lightweight UAV configuration still showed a 2.2 mm gauge discrepancy relative to TLS, the laboratory validation and the strong performance of optimized acquisitions indicate that tolerance-compliant railway parameter extraction may be achievable with higher-end UAV platforms and improved rail-side visibility. Overall, the results confirm the strong potential of UAV photogrammetry for near-industrial railway documentation.

1. Introduction

Accurate geometric documentation of railway infrastructure is essential for construction, maintenance, and safety management. Traditionally, this documentation relies on high-precision terrestrial surveys using total stations, laser scanning, or dedicated measurement trains. While these methods can achieve millimeter accuracy, they are time-consuming, costly, and operationally disruptive, often requiring track closures or night operations to avoid interference with active rail traffic. At the same time, the growing need for rapid, cost-effective, and high-resolution spatial data has driven increasing interest in Unmanned Aerial Vehicle (UAV)-based measurement systems for infrastructure monitoring (Chen et al., 2019). UAV photogrammetry, when properly implemented, can deliver dense, accurate, and repeatable 3D data over large areas with minimal operational downtime (De Winter et al., 2022) (Fig 1.).

Compared to conventional ground-based measurements (Fig. 2), UAV-based photogrammetry offers several potential advantages: flexible deployment without direct track access, reduced survey time, and improved operator safety. However, the technique faces critical challenges in achieving the millimeter-level precision required for rail infrastructure analysis. The attainable accuracy is limited by flight altitude and obliqueness restrictions imposed by local aviation regulations, image geometry and Ground Sampling Distance (GSD) constraints, and the difficulty of establishing reliable ground control in linear, repetitive railway environments. Furthermore, surface reflectivity of rails, variable lighting, and UAV platform stability introduce photogrammetric uncertainties that can degrade point cloud precision and reliability (Ait-Lamallam et al., 2025). Consequently, while UAV imagery has proven effective for centimeter-level mapping, its feasibility for detailed rail parameter extraction, such as gauge, slope and cant, remains largely unverified.

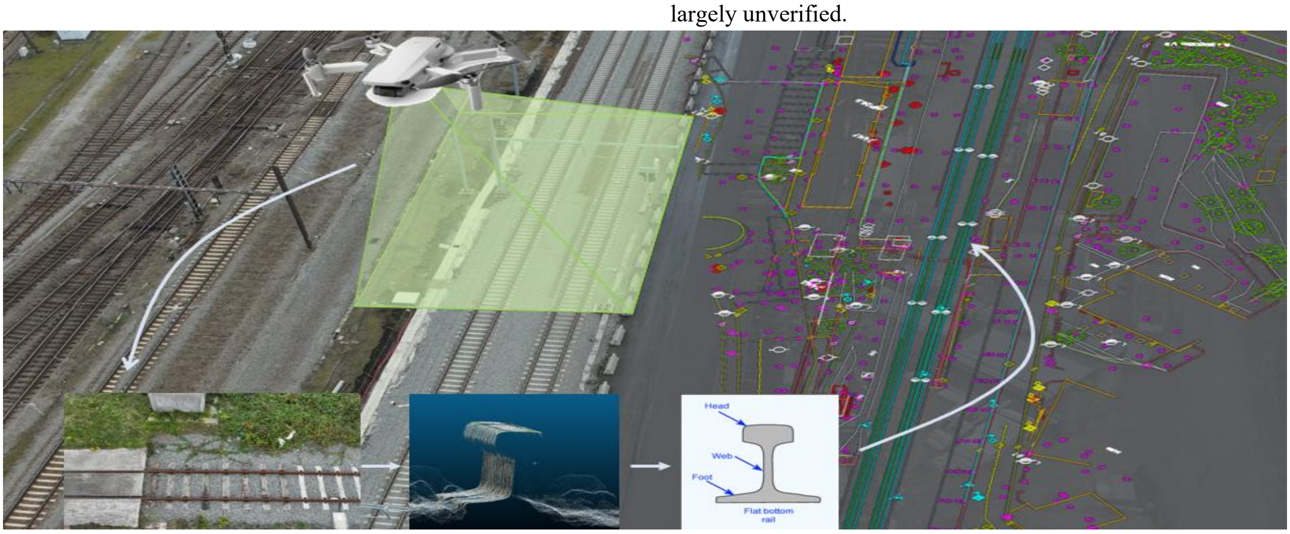

Figure 1: Overview of the proposed railway parameter evaluation framework using RTK-enabled high-precision UAV-photogrammetry.

Figure 2: (left) Conventional GEDO survey trolley system, (middle) unconstrained UAV flight image (A=5 m, GSD=2 mm) and (right) constrained conventional flight image (A=30m, GSD=11 mm).

This study presents a feasibility assessment of extracting rail system parameters from high-precision UAV photogrammetry, aiming to bridge the gap between traditional surveying accuracy and UAV-based efficiency. We evaluate whether structure-from-motion (SfM) and multi-view stereo (MVS) procedures applied to aerial imagery can achieve the required absolute and relative accuracies for rail geometry assessment under varying flight constraints. Specifically, the research investigates the influence of flight altitude, camera angle, and regulatory limitations on achievable point cloud quality and geometric reliability. The study compares unconstrained and constrained flight scenarios against total station and laser scanning ground truth data to determine compliance with railway accuracy standards. Ultimately, the work aims to define optimized UAV flight parameters and processing strategies that can bring UAV-based railway documentation closer to operational readiness and market adoption.

2. Related Work

2.1 UAV Flight Geometry and 3D Reconstruction Accuracy

The geometric configuration of UAV flight missions, as defined by the flight altitude, image overlap, camera angle, and network layout, plays a critical role in determining the achievable accuracy of 3D reconstruction. The GSD, controlled primarily by the combination of flight altitude and camera sensor specifications, sets the theoretical resolution of the resulting dataset, while image network geometry determines whether this accuracy can be realized (Rupnik et al., 2021). Studies consistently show that, under optimal imaging geometry with sufficient ground control or direct georeferencing, accuracies typically range from one to three times the GSD (Martínez-Carricondo et al., 2023; Štroner et al., 2021).

However, corridor-style flight missions, typical for linear infrastructure such as railways, pose specific challenges. Limited cross-track overlap and parallel flight paths can induce systematic deformations, known as the “bowl” or “dome” effects, resulting in vertical distortions of up to several decimeters when the image block geometry is poorly constrained (Ait-Lamallam et al., 2025). These effects can be mitigated through multi-directional or cross-flight configurations, as well as by incorporating oblique imagery to strengthen network geometry (Maboudi, 2021, Gerke et al., 2016, McMahon et al., 2021).

When RTK or PPK-based direct georeferencing is applied, the absolute accuracy of individual camera positions can reach 20-30 mm, outperforming conventional differential GNSS (Gerke et al., 2016, Žabota et al., 2021). Typical UAV-based infrastructure surveys with GSDs between 1 and 10 mm achieve altimetric RMSEs of 10-30 mm (Ferrer-González et al., 2020), while optimized RTK-supported flights, particularly those using cross-flight or oblique imaging, can achieve planimetric accuracies below 10 mm for 1-2 mm GSDs (Štroner et al., 2021). Overall, these studies establish that the relationship between flight geometry and reconstruction accuracy is governed by both image scale (GSD) and the degree to which block geometry constrains depth estimation.

2.2 3D Reconstruction Accuracy

High-precision UAV photogrammetry has increasingly been validated for infrastructure inspection, including railway and corridor documentation, revealing that UAV-photogrammetry can achieve millimeter-level precision. The closest related works to railway reconstruction are the following: (Ghassoun et al., 2021) reported root mean square errors (RMSEs) of 3 mm in planimetry and 8 mm in altimetry compared to total station benchmarks at 0.9 mm GSD using robust RTK-positioning. (Dunthorne et al., 2018) achieved 3D measurement accuracies up to 5 mm for railway infrastructure with GSDs of 1-2 mm with their Vogel R3D platform, equipped with a 100 MP sensor. (Ćmielewski et al., 2021) achieved accuracies of 1.2 mm in planimetry, and 1.3 mm in altimetry when monitoring crane tracks at flight heights of 10-30 m. These works show that the required accuracy (1-2 mm) is most likely obtainable at lower flight altitudes, but current still too high (5-8 mm) for railway documentation for the conventional 30 m flight altitude.

Comparable accuracy levels have been reported for other linear infrastructure: (Ferrer-González et al., 2020) obtained planimetric RMSEs below 31 mm and altimetric RMSEs below 81 mm for a 2.1 km road corridor (GSD = 17.5 mm), demonstrating that the accuracies indeed correspond to one to three times the GSD. Other studies confirm this trend across varied environments. (Gerke et al., 2018) reported RMSEs of 20 mm in planimetry and 30 mm in altimetry for photogrammetric image blocks of stockpiles. (Ruzgienė et al., 2015) obtained an average deviation of 29 mm for road surface modeling, and recorded altitude accuracies of 22 mm in urban road mapping. (Liu et al., 2018) achieved 30-40 mm accuracy for urban image blocks with 16 mm GSD.

Several studies have also examined how accuracy scales with flight parameters and control configuration. (Martínez-Carricondo et al., 2023) showed that increasing the number of ground control points significantly improves planimetric precision, while higher flight altitudes tend to increase horizontal error. However, (Štroner et al., 2021) achieved sub-30 mm accuracy using RTK-enabled flights without ground control, reinforcing that direct georeferencing can ensure stable results in constrained environments. We have confirmed this in prior work, where we obtained ~15mm inter-distances on artificial targets (Cuypers et al., 2023, Bartczak et al., 2023).

https://doi.org/10.5194/isprs-archives-XLIX-B2-2026-387-2026

Alternative sensing modalities, such as UAV laser scanning (Dreier et al., 2021), can achieve RMSEs below 20 mm in planimetry and 40 mm in altimetry compared to terrestrial laser scanning (TLS). However, these systems are typically heavier, costlier, and restricted by (national) flight regulations (such as by the European Union Aviation Safety Agency (EASA) and Belgian Civil Aviation Authority). Consequently, UAV-based photogrammetry remains a the most promising and practical method for high-accuracy railway documentation, balancing precision, operational efficiency, and regulatory compliance.

Beyond point cloud analysis, high-resolution UAV imagery itself can be used to extract relative rail geometry through direct line detection and matching on the images (i.e. HED). This approach avoids the additional accuracy loss associated with 3D reconstruction, as measurements are made directly in image space. However, it requires precise identification of the rail edges and consistent line pairing across images. In our previous work, (Cuypers et al., 2023) demonstrated that such line-based methods achieve accuracies of approximately 2×GSD, corresponding to 2.3 mm when using a 100 MP camera at 30 m altitude (1.17 mm GSD). While effective for gauge deviation, this technique cannot recover full 3D parameters such as alignment, cant or twist, and is therefore complementary to point cloud–based reconstruction rather than a replacement (Bassier et al., 2024).

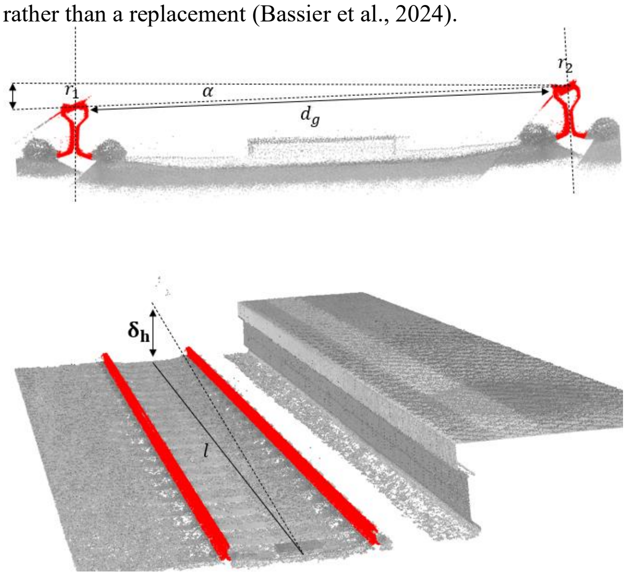

Figure 3: Railway parameters including cant (α), twist (δ_α), gauge (+ variation) (d) and rail axis (l).

2.3 Railway parameters

In Belgium, the geometric integrity of railway tracks is governed by a well-defined set of parameters that describe the position, orientation, and relative alignment of both rails. See Table 1 for the 220 km/h < V ≤ 300 km/h (most strict) category (Fig. 3).

Table 1: Track geometry param. and Belgian tolerances (2σ) reported every 0.5m, for new constructions in the highest category 220 km/h < V ≤ 300 km/h.

Parameter	**Definition**	**Nominal Value**	**Tolerance (2σ)**
Gauge	Distance between the inner faces of both rails, 14 mm below the top of the railhead	1463 mm	2 mm
Alignment	Horizontal deviation of the rail axis from the design centerline	—	2 mm / 10 m
Level (Longitudinal profile)	Vertical deviation of railhead elevation along the track	—	2 mm / 10 m
Cant	Difference in height between left and right railheads	—	2 mm
Twist	Variation in cant per 3/6/9 m	—	0.7 mm per m
Gauge variation (local)	Local change in gauge over 1 m	—	1 mm
Track axis position (absolute)	Absolute position of track centerline	—	Alt: 10 mm Plan: 5 mm

Conventional surveying methods, such as total station (TS) measurements, have historically been employed to assess these parameters at discrete intervals along the track. Under standard field conditions, TS achieve 1-2mm absolute tolerances (2σ) over short baselines, and this can be increase about tenfold using a calibrated GEDO and ATR tracking, making them the reference method for geometry control and calibration (Fig. 4).

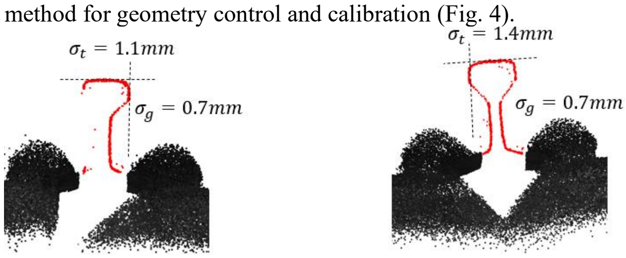

Figure 4: Ground truth laser scanning accuracies on rail section (0.5 m) using Leica RTC360 with σ_{3d} = 1.9 mm / 10 m.

2.4 Flight regulations

Under the European EASA framework (Regulations EU 2019/947 and 2019/945), UAV operations in Belgium are governed by the Belgian Civil Aviation Authority (BCAA) and the Droneguide geozone system. Railway surveys typically operate in the *Open Category*, which allows flights up to 120 m AGL, provided operations remain within visual line of sight (VLOS) and maintain a 30 m horizontal distance from uninvolved persons (subcategory A2). The general 150 m separation from residential or industrial areas (A3) is waived for Infrabel-authorized operations, which fall under a *Specific Category* exemption allowing corridor flights directly above the railway right-of-way, as otherwise flights in urban areas are not possible. Infrabel’s operational safety guidelines state that the minimum flight height above the rail level (RL) must ensure obstacle clearance for catenary systems (7-12m) for safety and to prevent electromagnetic interference. In XY, a 5m clearance from the rail axis is recommended, again for safety reasons and to prevent wake turbulence. These regulatory constraints directly affect attainable image geometry and GSD, dictating both flight altitude and permissible obliqueness during UAV-based railway documentation.

3. Methodology

The methodology of this study is structured around two main objectives: (1) maximizing the geometric accuracy and completeness of the reconstructed point cloud, and (2) testing the precision of rail parameter extraction derived from that 3D data. Together, these steps aim to establish an operational framework that balances safety, efficiency, and accuracy within the constraints of Belgian and European UAV regulations.

3.1 Maximizing Point Cloud Accuracy and Coverage

The first stage aims to determine the flight configuration, camera setup, and photogrammetric processing strategy that yield the most accurate and complete 3D reconstruction of the railway corridor. The experiments evaluate the influence of flight altitude, image obliqueness, overlap, and sensor configuration on reconstruction quality. Three scenarios are considered.

1. **Controlled lab tests:** First, we assess whether SfM is intrinsically capable of millimetric reconstructions on reflective steel surfaces. To this end, a mock-up of two steel I-profiles was arranged to simulate the inner geometry of a rail pair, with the flange-to-flange distance used as an analogue for the gauge (Fig. 5). The use of gauge as validation metric is motivated by the fact that it depends on one of the smallest and most critical rail features and therefore provides a stringent test of relative geometric accuracy. A Leica P30 terrestrial laser scan served as geometric reference, while independent SfM reconstructions were generated from handheld Canon EOS 5D Mark II and DJI Mavic 3E image sets acquired in a circular imaging pattern ($0.3mm$ GSD).

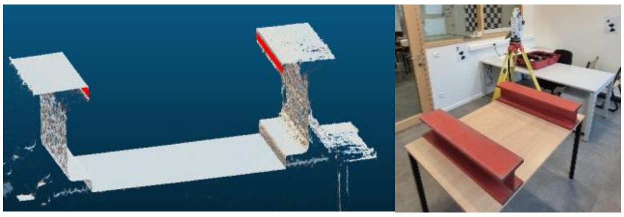

Figure 5: Controlled lab SfM with DJI Mavic 3E ($0.3mm$ GSD at $1-2$m).

2. **Open Category flights:** Second, we test standard operational conditions (≈ 30 m altitude, nadir imaging, and a minimum 30 m separation from uninvolved persons). These flights provide the realistic baseline for regulatory-compliant deployment, but are expected to offer limited visibility of the rail sides and reduced effective resolution on the gauge-relevant surfaces (Fig. 6).

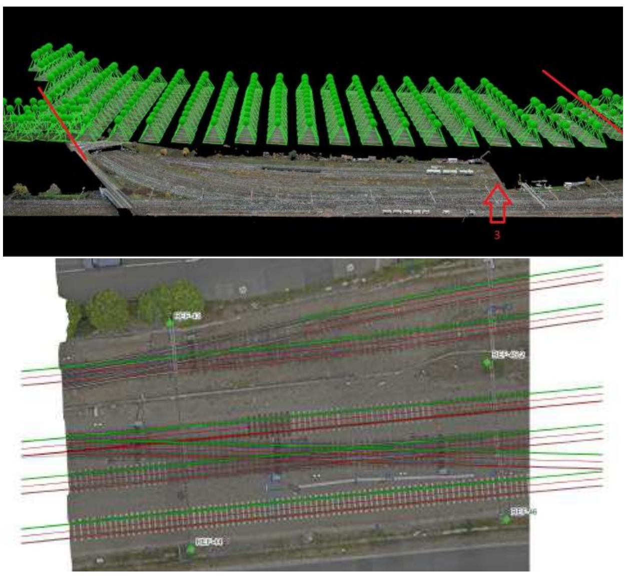

Figure 6: DJI Matrice 300 flights with 100 MP Phase One iXM camera (1.17mm GSD at 30 m), with projected rail axes.

3. **Optimized flights**: Third, we maximize reconstruction quality under controlled site conditions at three test locations. These missions exploit lower flight altitudes and stronger obliqueness to improve stereo geometry and side visibility of the rails. Specifically, we adopt 10-20 m altitudes (12m + safety zone) and a 5m planimetric buffer based on the minimal safety regulations, on a single- and double-track rail system. We use conventional 75% side and forward overlap and also include oblique side-trajectories (Fig. 7).

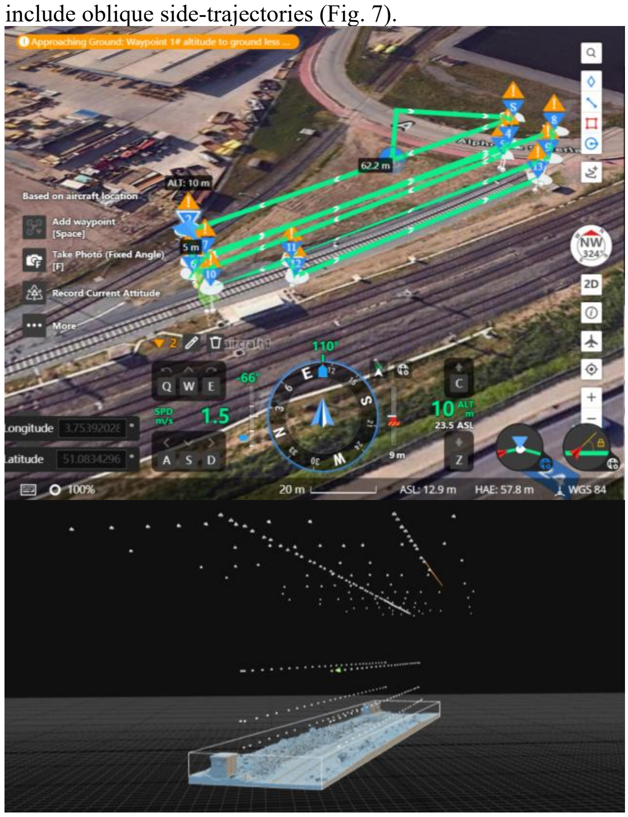

Figure 7: DJI Mavic 3E with flights between 2-5 m (maximum accuracy) and Open category flights (25-35 m above RL).

The missions employed two SOTA UAV platforms to evaluate the influence of sensor configuration and flight geometry on reconstruction quality:

A. **DJI Matrice 300**: This high-end system features a 100 MP Phase One iXM camera + RTK (11664 × 8750 px, f=100mm) with 1.17mm GSD at 30m.

B. **DJI Mavic 3 Enterprise (3E):** This system represents a lightweight, commercially accessible alternative to explore the maximum obtainable point cloud accuracy. It features a 20 MP 4/3″ camera + RTK (5280 × 3956 px) with a f=12mm lens.

In total, 6 configurations were evaluated and combined to study the accuracy: 1 in the lab and 5 on single/double tracks (Table2).

Table 2: Flights executed with DJI Matrice 300 (A) and Mavic 3E (B) UAV platforms.

ID	UAV	Alt.	GSD	Description / Purpose
F0	B + Canon	1-2 m	0.3-0.5 mm	High-resolution baseline dataset testing the maximum achievable accuracy
F1	A	30 m	1.17 mm	High-resolution baseline dataset conform Open Category restrictions; used to benchmark absolute and relative accuracy.

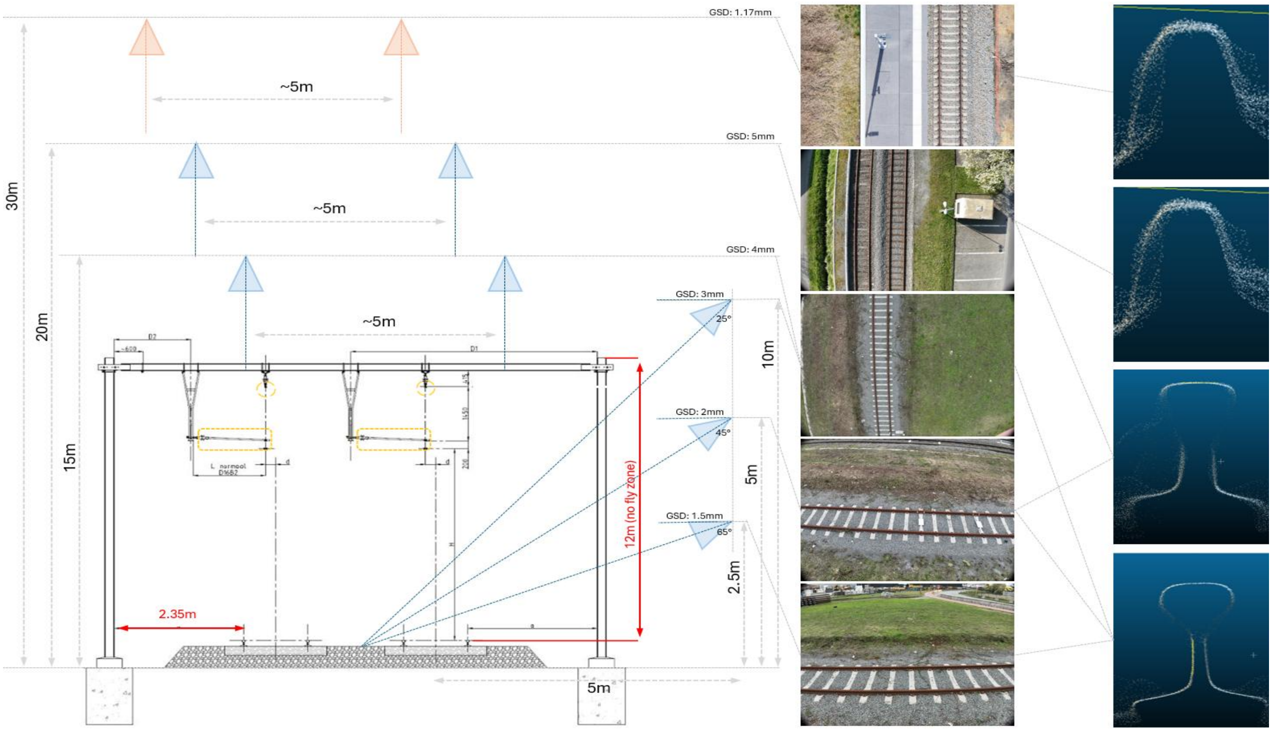

Figure 8: Schematic overview of the rail system flights using the DJI Matrice 300 (Orange) and DJI Mavic 3 Enterprise (Blue) including altitudes, XY distances, Nadir angle, GSD and the resulting point cloud reconstructions.

F2	B	20 m	5 mm	Low-cost equivalent Nadir flights over the tracks simulating Open Category
F3	B	15 m	4 mm	Medium-altitude Nadir flights over the tracks to maximize XY accuracy
F4	B	10 m	3 mm	Medium-altitude oblique side flights to increase Z accuracy
F5	B	5 m	2 mm	Low-altitude flight oblique side flight to improve overall reconstruction accuracy and coverage
F6	B	2.5 m	1.5 mm	Most extreme low-altitude side oblique flight to maximize Z accuracy & coverage.

3.2 Rail Parameter Extraction and Accuracy Evaluation

The next objective is to determine how closely UAV-based photogrammetry can reproduce the reference values obtained from total-station and TLS measurements.

3.2.1 Segmentation and Point Selection

To standardize the analysis, both the SfM and TLS point clouds were segmented into 0.5 m longitudinal rail sections. Over this limited length, the effect of track curvature can be neglected, allowing each segment to be treated as locally straight. For each rail, two geometric entities were extracted:

- **Railhead top surface $t \pm \sigma_t$**: A best-fit plane was estimated on the running surface of the railhead. This plane provides the local height reference and allows the vertical consistency of the reconstructed surface to be evaluated through its residuals.
- **Gauge reference $g \pm \sigma_g$:** In accordance with railway practice, gauge is evaluated **14 mm below the running surface**, i.e. on a plane parallel to the railhead top plane and shifted vertically by 14 mm. Points within a 2mm narrow band around this offset plane were selected, and only the inner-side points were retained for gauge estimation.

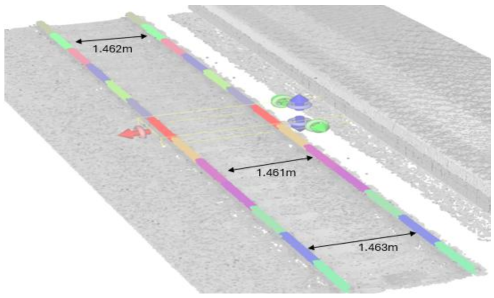

Figure 9: 0.5m sections extracted from the point cloud to determine rail parameters.

This segmentation strategy reduces sensitivity to single-point noise and yields more stable, repeatable measurements by fitting geometric primitives to many points rather than relying on individual samples (Fig. 9, 10).

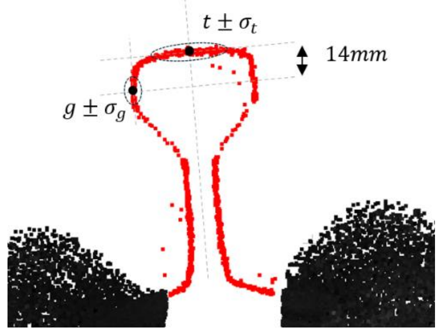

Figure 10: Extraction of vertical accuracy σ_t from the railhead, and the gauge reference accuracy σ_g 14mm below the railhead.

3.2.2 Parameter extraction

1) Gauge d_g + tolerance t_g:

Since the rails are near parallel, the gauge is computed as the averaged cross product between the centers of both gauge lines and their opposing gauge reference lines l(g):

$$d_g = ||(g_2 - g_1) \times l(g_2)||$$

With each gauge line determined by a best-fit 3D line obtained from the selected gauge-reference points.

The gauge tolerance t_g is driven by the uncertainty of the line fitting (RMSE on distances from fitted points) which is also a measure for the relative point accuracy. The tolerance (95% ~ 2σ) of the gauge should thus be lower than

$$t_g \geq 2\sqrt{\sigma_{g_1}^2 + \sigma_{g_2}^2} \approx 2\sqrt{2\sigma_g^2}$$

With

t_g=2mm
$\sigma_{g_1} \approx \sigma_{g_2} \approx \sigma_g \leq 0.7mm$

For this, we assume that the gauge accuracies on both sides are similar.

The tolerance for the local gauge variation $t_{g'}$ is analogously determined by two consecutive gauge measurements. Again assuming that gauge line fitting accuracies are consistent in the point cloud since the flight configurations are consistent, the tolerance level to clear is

$$t_{g'} \geq \sqrt{4\sigma_g^2}$$

With

$t_{g'}$=1mm
$\sigma_g \leq 0.5mm$

2) Track axis points $c \in C$: The track axis l is given by the polyline of control points $c \in C$ at the midpoint between g_1 and g_2:

$$c = \frac{1}{2}(g_1 + g_2)$$

The tolerance of the absolute positioning of the control points (Alt: 10 mm, Plan: 5 mm) is entirely driven by GNSS accuracies, and the marking of control points on the catenary poles along the track. For this study, we forego this analysis and instead first focus on the feasibility of achieving high local relative accuracy.

3) Level δ_h + tolerance t_h: The height difference between two railheads is given by the height difference between both planes fitted through similar points on the top of the railhead t_1, t_2.

$$\delta_h = |t_{z_1} - t_{z_2}|$$

With the tolerance being

$$t_h \geq 2\sqrt{\sigma_{t_1}^2 + \sigma_{t_2}^2}$$

With

t_h=2mm
$\sigma_t \leq 0.7mm$

4) Cant α + tolerance t_α: Logically, the cant tolerance is equal to the level tolerance since it is also computed using the top of the railheads.

$$t_\alpha \sim t_h \rightarrow \sigma_t \leq 0.7mm$$

Twist, i.e. the variation of cant over distance, is calculated similarly to the gauge variation but with a stricter tolerance.

$$t_{c'} \geq \sqrt{4\sigma_{t_h}^2}$$

With

t_h=0.7mm
$\sigma_t \leq 0.35mm$

4. Experiments

Two preliminary experiments were conducted to evaluate whether the tested image-acquisition configurations provide sufficient local precision for railway parameter extraction. Rather than reporting every railway parameter separately, the analysis focuses on the two governing local precision terms introduced in Section 3.2: the vertical railhead precision σ_t and the gauge-reference precision σ_g. If the following conditions are satisfied

$$\boldsymbol{\sigma_t \leq 0.35mm \wedge \sigma_g \leq 0.5mm}$$

Then the reconstructed point cloud is, in principle, precise enough to support the full set of relative rail parameters, including gauge, cant and twist.

All photogrammetric datasets were processed with the same RealityScan SfM–MVS workflow at the highest quality settings, such that differences in the results can be attributed primarily to flight geometry, GSD, and image coverage rather than to processing choices. Where possible, the datasets were constrained by Total station-control, thus suppressing any scaling issues.

Where a TLS reference was available (Leica P30), the local precision criteria were complemented by an independent comparison of the reconstructed gauge distance against TLS.

4.1 Laboratory validation

The laboratory results in Table 3 and Fig. 11 show that the individual point accuracies σ_p of the UAV (RMSE of planefitting) range between 0.49 mm (right) and 0.97 mm (left). This is extremely promising since the accuracy of the gauge references $\{g_1, g_2\}$ is theoretically given by the point accuracy divided by the redundancy of the plane fitting.

$$\sigma_g = \sqrt{\frac{\sigma_p^2}{n}}$$

With

$n \approx 36$

Which is circa three times better than the required accuracy. However, the difference between both flanges indicates that there are also systematic errors present. Especially the left flange had a lower accuracy due to reflections.

Table 3: Flange gauge point ($\sigma_{p_1}, \sigma_{p_2}$) and plane ($\sigma_{g_1}, \sigma_{g_2}$) accuracies in lab conditions in mm.

Datasets (mm)	σ_{p_1}	σ_{g_1}	σ_{p_2}	σ_{g_2}	d_g
Mavic 3E	0.97	**0.16**	0.49	**0.08**	614.85
Canon EOS 5D	0.65	**0.11**	0.39	**0.07**	614.16
TLS	0.30	**0.05**	0.30	**0.05**	614.54

https://doi.org/10.5194/isprs-archives-XLIX-B2-2026-387-2026

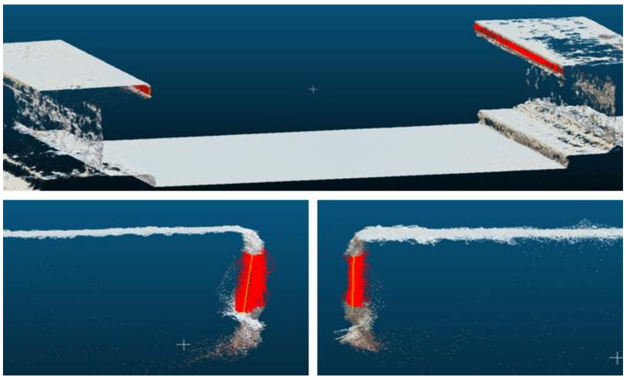

Figure 11: DJI 3E flange plane estimation, with twice as high noise values on the g_1(left) due to specular flight reflections.

This is confirmed by the inter-distance comparison of the systems i.e.

$$\delta_{TLS\rightarrow Canon} = 0.38mm$$
$$\delta_{Canon\rightarrow 3E} = 0.69mm$$
$$\delta_{TLS\rightarrow 3E} = 0.31mm$$

Which is nearly twice as high than the expected accuracy of the distance comparisons $\sigma_{\delta d_g}$(not impossible but highly unlikely).

$$\sigma_{\delta d_g} = \sqrt{\sigma^2_{g_{1,TLS}} + \sigma^2_{g_{2,TLS}} + \sigma^2_{g_{1,3E}} + \sigma^2_{g_{2,3E}}} \approx 0.19mm$$

This leads us to conclude that (i) we best report both the point and plane accuracies for σ_t *and* σ_g since the representative accuracy is somewhere in between. (ii) The SfM is capable of achieving the required precision under controlled conditions.

4.2 Field experiments: local surface precision

The field experiments then tested how the rail-surface fit precision changes with flight geometry. First of all, the conventional (unoptimized) flights including F2 and F3 Nadir flights at 20 and 15 m failed to produce an adequate rail profile (Fig. 12).

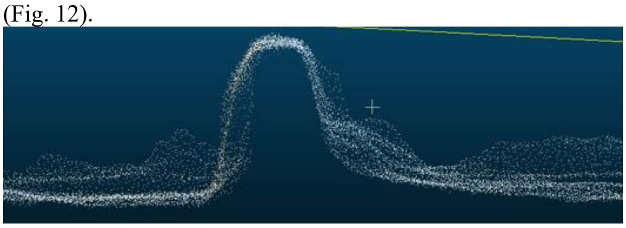

Figure 12: F2 & F3 Open category Nadir 20 – 15m flights (GSD= 4-5 mm): NA due to unrecognizable points.

Second, by adding the side-looking F5 (5m, GSD = 2mm) flight to F3, we could recover a first usable rail profile. Analogous to the lab tests, we distinguish between the point accuracies derived from the plane fitting (top $\sigma_{p_t} = 0.4mm$, gauge $\sigma_{p_g} = 1.1mm$) and the plane accuracies themselves (top $\sigma_t = 0.06mm$, gauge $\sigma_g = 0.18mm$) (see Table 4). Noticeably, the top of the rail is reconstructed nearly three times more accurate than the gauge.

Table 4: Railhead and gauge point ($\sigma_{p_t}, \sigma_{p_g}$) and plane ($\sigma_t, \sigma_g$) accuracies during field tests in mm.

Dataset (mm)	σ_{p_t}	σ_t	σ_{p_g}	σ_g	d_g
Requirements	-	**0.35**	-	**0.5**	-
F2/F3	-	-	-	-	-
F5+F3	0.40	**0.06**	1.10	**0.18**	-
F3+F4+ F5+F6	0.25	**0.04**	0.72	**0.12**	1436.9
TLS	0.30	**0.05**	0.30	**0.05**	1434.7

This is to be expected since it is less sensitive to varying light conditions, is a larger surface, and is seen from a better vantage point. From the results, we can conclude that also during this field test, we most likely achieve the required accuracy as both plane accuracies are well below the expected values. However, the profile is not very clear, so automatically selecting the correct reference points might prove challenging.

Third, if we include all side-looking flights i.e. F4 (10m), F5(5m) and F6 (2.5m), we achieve up to 40% more accurate results. As the flight at 10m probably does not add much to the accuracy, we conclude that the best performing flights consist of Nadir flights at 15m + side-looking flights at 2.5 and 5m (Fig. 13).

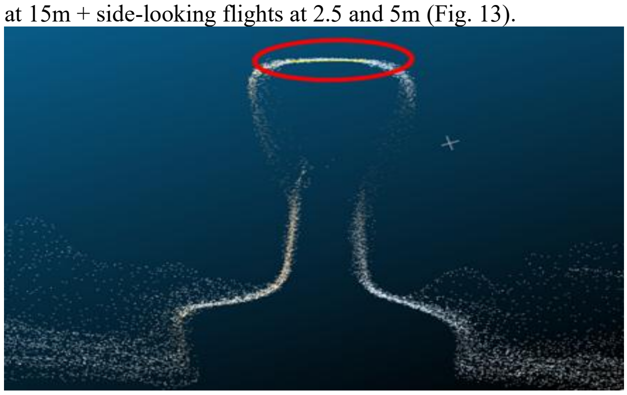

Figure 13: Optimized flight including Nadir F2 (20 m) + side-looking flight F5 (5m, GSD = 2mm) resulting in $\sigma_t =$ **[0.06mm; 0.4mm]** and $\sigma_g =$ **[0.18mm; 1.1mm]**.

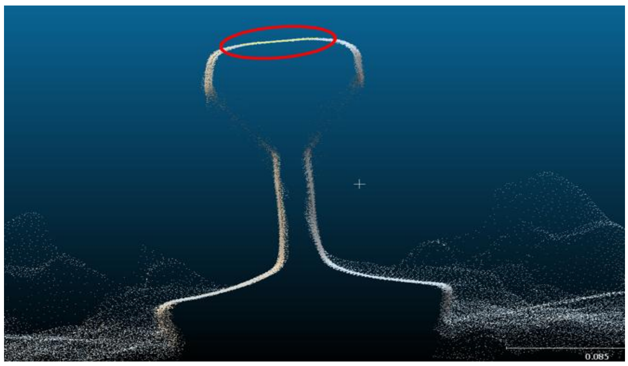

Figure 14: Best possible flight including Nadir F2 (20m) + side-looking flights F4 (10m) + F5 (5m) +F6 (2.5m), resulting in $\sigma_t =$ **[0.04mm; 0.25 mm]** and $\sigma_g =$ **[0.12mm; 0.72mm]**.

We again compared this result against the TLS, but here we found a discrepancy of 2.2 mm between the gauge measurements in both datasets. This is surprising and cannot be explained by both the expected point-based RMS and plane-fit precision, since it is more than twice as large.

$$0.14mm\ (plane) \leq \sigma_{\delta d_g} \leq 0.87mm(points)$$

When inspecting both profiles (Fig.15), we observed slight curvature deviations and increased noise levels in the SfM reconstruction, but no evidence of faulty depth estimation. As such, this suggests a systematic reconstruction or registration error, likely related to the sensitivity of the side geometry to opposing-view matching which is especially sensitive in railway scenes. Other possible explanations, such as a scaling/rotation of the SfM project due to the low RTK-GNSS (15mm) accuracy, is unlikely since its effect is near-zero due to the large quantity of GNSS measurements and size of the recorded sites (>60m).

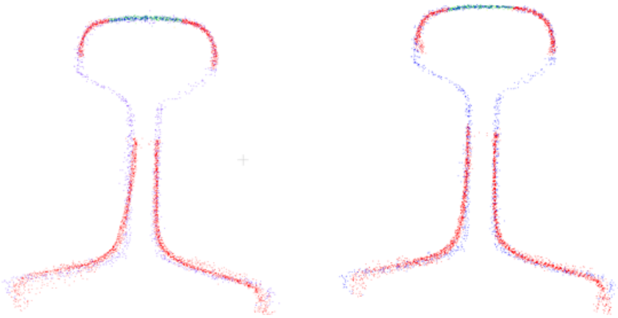

Figure 15: Overlay of TLS (blue) with the best flight configuration (F2 + F4 + F5 + F6) (red).

5. Conclusion

This study evaluated the feasibility of UAV-based SfM photogrammetry for high-precision railway measurement under both controlled and operational conditions. The results show that, in laboratory conditions, the method can achieve sub-millimetre inter-distance agreement and is therefore intrinsically capable of recovering rail-like geometry with very high relative precision. In field conditions, optimized low-altitude side-looking acquisitions substantially improve rail reconstruction compared with standard nadir flights, confirming that flight geometry is the main factor controlling local accuracy and coverage. However, despite these promising results, the best field configuration still showed a 2.2 mm discrepancy in gauge with respect to TLS, indicating that full compliance with the strictest railway tolerances is not yet proven. Overall, the work demonstrates that UAV-SfM is a promising and operationally flexible approach for railway documentation, but further refinement is still required to robustly reconstruct the narrow rail-side geometry needed for tolerance-compliant parameter extraction.

Acknowledgements

This work was made possible with Infrabel, TUC Rail and De Witte Vandecaveye dat. It was funded by FWO Strategic base research (1S43224N), and internal KUL Geomatics Funding.

References

Ait-Lamallam, S., Lamrani, R., Mastari, W., & Kechna, M. (2025). Effective strategies for mitigating the "bowl" effect and optimising accuracy: A case study of UAV photogrammetry in corridor projects. *Drones*, *9*(6), 387. https://doi.org/10.3390/drones9060387

Bassier, M., J. Vermandere, S. De Geyter, and H. De Winter, (2024). GEOMAPI: Processing Close-Range Sensing Data of Construction Scenes with Semantic Web Technologies. *Automation in Construction* 164: 105454, https://doi.org/10.1016/j.autcon.2024.105454

Bartczak, E., Bassier, M., and Vergauwen, M. (2023) Proceedings In Uas-Assisted Bridge Inspections: Rtk-Based Photogrammetric Reconstruction And Spatial Filtering, *ISPRS Archives of the Photogrammetry, Remote Sensing and Spatial Information Sciences, https://doi.org/10.5194/isprs-archives-XLVIII-1-W2-2023-1873-2023*

Chen, S., Laefer, D.F., Mangina, E., Zolanvari S.M.I., Byrne J. (2019). UAV Bridge Inspection through Evaluated 3D Reconstructions. J. Bridge Eng. 24. https://doi.org/10.1061/(ASCE)BE.1943-5592.0001343

Cuypers, S., De Winter, H., Bassier, M., & Vergauwen, M. (2023). Planimetric Rail Positioning Using Uav Photogrammetry: Towards Automated And Safe Railway Infrastructure Monitoring, *ISPRS Archives of the Photogrammetry, Remote Sensing and Spatial Information Sciences*, https://doi.org/10.5194/isprs-archives-XLVIII-1-W2-2023-589-2023

Ćmielewski, K., Gołuch, P., Kuchmister, J., Wilczyńska, I., Ćmielewski, B., & Grzeja, O. (2021). Detection of crane track geometric parameters using UAS. *Remote Sensing*, *13*(15), 2987. https://doi.org/10.3390/rs13152987

De Winter, H., Bassier, M., & Vergauwen, M. (2022). Digitisation in road construction: Automation of as-built models. *The International Archives of the Photogrammetry, Remote Sensing and Spatial Information Sciences, 46*, 69–76. https://doi.org/10.5194/isprs-archives-XLVI-5-W1-2022-69-2022

Dreier, A., Janßen, J., Kuhlmann, H., & Klingbeil, L. (2021). Quality analysis of direct georeferencing in aspects of absolute accuracy and precision for a UAV-based laser scanning system. *Remote Sensing*, *13*(18), 3564. https://doi.org/10.3390/rs13183564

Dunthorne, J. (2018). Improving rail infrastructure inspection efficiency with aerial data acquisition for a digital railway. *GIM International*, *32*(2–3), 24–26.

Ferrer-González, E., Agüera-Vega, F., Carvajal-Ramírez, F., & Martínez-Carricondo, P. (2020). UAV photogrammetry accuracy assessment for corridor mapping based on the number and distribution of ground control points. *Remote Sensing*, *12*(15), 2447. https://doi.org/10.3390/rs12152447

Gerke, M. (2016). Accuracy analysis of photogrammetric UAV image blocks: Influence of onboard RTK-GNSS and cross flight patterns. *ISPRS Archives of the Photogrammetry, Remote Sensing and Spatial Information Sciences*, *XLI-B1*, 827–833. https://doi.org/10.5194/isprsarchives-XLI-B1-827-2016

Gerke, M. (2018). Accuracy assessment of UAV photogrammetry for stockpile modeling. *ISPRS Archives of the Photogrammetry, Remote Sensing and Spatial Information Sciences*, *XLII-2*, 383–390. https://doi.org/10.5194/isprs-archives-XLII-2-383-2018

Ghassoun, Y., Colomina, I., Molina, P., & Blázquez, M. (2021). Implementation and validation of a high-accuracy UAV photogrammetry-based rail track inspection system. *Remote Sensing*, *13*(3), 384. https://doi.org/10.3390/rs13030384

Liu, Y. (2018). Generating a high-precision true digital orthophoto map based on UAV images. *ISPRS International Journal of Geo-Information*, *7*(3), 98. https://doi.org/10.3390/ijgi7030098

Martínez-Carricondo, P., Agüera-Vega, F., & Carvajal-Ramírez, F. (2023). Accuracy assessment of RTK/PPK UAV-photogrammetry projects using differential corrections from multiple GNSS fixed base stations. *Geocarto International*, *38*(1), 1–17. https://doi.org/10.1080/10106049.2023.2197507

McMahon, C., Mora, O. E., & Starek, M. J. (2021). Evaluating the performance of sUAS photogrammetry with PPK positioning for infrastructure mapping. *Drones*, *5*(2), 50. https://doi.org/10.3390/drones5020050

Mehdi Maboudi. (2021). Improving the internal accuracy of UAV-image blocks using local low-altitude flights and scale bars. *ISPRS Archives of the Photogrammetry, Remote Sensing and Spatial Information Sciences*, *XLVI-M-1-2021*, 125–132. https://doi.org/10.5194/isprs-archives-XLVI-M-1-2021-125-2021

Rupnik, J., Nex, M., & Remondino, F. (2021). Oblique multi-camera systems for corridor mapping: Accuracy assessment and processing challenges. *ISPRS Journal of Photogrammetry and Remote Sensing*, *174*, 1–14.

https://doi.org/10.1016/j.isprsjprs.2021.02.001

Ruzgienė, B., Aksamitauskas, Č. V., Daugėla, I., Prokopimas, Š., Puodžiukas, V., & Rekus, D. (2015). UAV photogrammetry for road surface modelling. *The Baltic Journal of Road and Bridge Engineering*, *10*(2), 151–158. https://doi.org/10.3846/bjrbe.2015.19

Štroner, M., Urban, R., Seidl, J., Reindl, T., & Brouček, J. (2021). Photogrammetry using UAV-mounted GNSS RTK: Georeferencing strategies without GCPs. *Remote Sensing*, *13*(7), 1336. https://doi.org/10.3390/rs13071336

Žabota, B., & Kobal, M. (2021). Accuracy assessment of UAV-photogrammetric-derived products using PPK and GCPs in challenging terrains: In search of optimized rockfall mapping. *Remote Sensing*, *13*(19), 3812. https://doi.org/10.3390/rs13193812